**RAA 2021** Vol. **21** No. **5**, 126(8pp) doi: 10.1088/1674-4527/21/5/126

*http://www.raa-journal.org* *http://iopscience.iop.org/raa*

***R**esearch in*
***A**stronomy and*
***A**strophysics*

# Magneto-acoustic waves in magnetic twisted flux tubes

Wei Wu[1,2], Robert Sych[2,3], Jie Chen[2] and Jiang-Tao Su[2,1⋆]

[1] School of Astronomy and Space Sciences, University of Chinese Academy of Sciences Beijing 100049, China
[2] Key Laboratory of Solar Activity, National Astronomical Observatories, Chinese Academy of Sciences, Beijing 100101, China; *sjt@nao.cas.cn*
[3] Institute of Solar-Terrestrial Physics SB RAS, Irkutsk 664033, Russia

Received 2020 November 30; accepted 2021 January 8

**Abstract** At present, many works about MHD wave diagnostics in magnetic flux tubes are based on some pioneering works not considering the contributions of magnetic twist. Other works considered the effect on MHD waves, but the dispersion relationship they presented only gave the wave modes of $m = 0, 1, 2...$ The kink mode of $m = -1$ was absent. Therefore, in this work we present a complete dispersion relationship that includes both magnetic twist and the wave mode of $m = -1$. Analogous to the $m = +1$ wave mode, the mode of $m = -1$ also exhibits the mode change at finite $kr_0$, from body to surface mode. The phase speeds of this mode are usually less than those of $m = +1$ mode. The harmonic curves of $m = \pm 1$ modes in dispersion relationship diagrams are approximately symmetric in respect to a characteristic velocity, e.g. the tube velocity in flux tubes. Based on the present dispersion relationship, we revisit the issue of spiral wave patterns in sunspots and find that the magnetic twist has no great influence on their morphology in the frame of linear perturbation analysis.

**Key words:** Sun: sunspots — Sun: oscillations — Sun: atmosphere

## 1 INTRODUCTION

In the context of MHD linear theory, wave propagation in untwisted magnetic flux tubes embedded in a magnetic environment was investigated by Edwin & Roberts (1983). The dispersion relations they derived have become a fundamental reference for the magneto-seismological inversion to probe the solar plasma. Later, Bennett et al. (1999) extended their work and studied wave propagation in the twisted magnetic flux tubes in an incompressible medium. Due to the twist introduced, the hybrid (surface-body) modes of oscillation appear in contrast to the case of an untwisted incompressible tube. Sausage ($m = 0$) MHD wave propagation in incompressible (Erdélyi & Fedun 2006) and compressible (Erdélyi & Fedun 2007) magnetically twisted flux tubes was investigated further. More recently, Erdélyi & Fedun (2010) studied the oscillatory modes of a magnetically twisted compressible flux tube in cylindrical geometry, and a general dispersion equation obtained in terms of Kummer functions for the approximation of weak and uniform internal twist.

However, it should be pointed out that Bennett et al. (1999) and Erdélyi & Fedun (2010) only presented the dispersion relationship diagrams (phase-speed diagrams of MHD oscillation modes) for the $m = +1$ mode of oscillation that will increase the twist in the tube. However, neither of them presented the $m = -1$ one of oscillation. This is because that the $m = 1$ mode is the more unstable of the two since the helical perturbation formed is of the same sense as the twist (Bennett et al. 1999). With more advanced astronomical instruments put into service, more fine structures of MHD waves on the Sun are detected, e.g. the armed-spiral wavefronts in the umbrae of sunspots (e.g., Sych & Nakariakov 2014; Su et al. 2016; Sych et al. 2020). They are likely created by the superposition of non-zero azimuthal modes driven 1600 km below the photosphere in the sunspots (Kang et al. 2019). For example, the one-armed pattern is produced by the slow-body sausage ($m = 0$) and kink ($m = 1$) modes. Naturally, we wander what the wave pattern looks like if magnetic twist is included in the flux tubes or the $m = -1$ mode is in place of that of $m = +1$. This is our motivation to complete the dispersion relationship diagram by including the $m = -1$ mode.

⋆ Corresponding author

In this paper, we attempt to give a general dispersion equation for the $m = -1$ oscillation mode in Section 2. Complete diagrams of the dispersion relations are described in Section 3 and the modeling of spiral wave patterns in Section 4. Finally, we conclude in Section 5.

## 2 GENERAL DISPERSION EQUATION OF THE ALLOWED EIGENMODES

### 2.1 Magnetic Twisted Flux Tube Model

We consider the modes of oscillation of a compressible magnetized twisted flux tube embedded within a uniformly magnetized plasma environment in cylindrical geometry $(r, \theta, z)$ (Erdélyi & Fedun 2010). In equilibrium, the plasma and magnetic field pressure satisfy the condition in the radial direction

$$\frac{d}{dr}(p_0 + \frac{B_0^2}{2\mu}) = -\frac{B_{0\theta}^2}{\mu_0 r}. \tag{1}$$

Here $B_0 = (B_{0\theta}^2 + B_{0z}^2)^{\frac{1}{2}}$ denotes the strength of the equilibrium magnetic field and $\mu_0$ is the magnetic permeability. The plasma density is taken to be uniform.

### 2.2 Dispersion Equation

A general dispersion equation has been obtained in terms of Kummer functions for the magneto-acoustic waves in the compressible magnetized twisted flux tubes (Erdélyi & Fedun 2010), which is

$$D_{\rm e}\frac{r_0}{m_{0\rm e}}\frac{K_m(m_{0\rm e}r_0)}{K'_m(m_{0\rm e}r_0)} = -\frac{A^2r_0^2}{\mu_0^2} + D_{\rm i}r_0^2\frac{(1-\alpha^2)}{m(1-\alpha)+2x_0\frac{M'(a,b,x_0)}{M(a,b,x_0)}}, \tag{2}$$

where the subscripts i and e respectively represent the interior and exterior of the tube, and $r_0$ is the radius of the tube, $m$ is azimuthal order of the mode, $b = m + 1$, $A$ is arbitrary constant, $K_m$ is the modified Bessel functions of the second kind, $K'_m$ is its derivative, $M(a, b, x_0)$ is the Kummer function evaluated at $x = x_0$, $M'(a, b, x_0) = \frac{a}{b}M(a + 1, b + 1, x_0)$ is its derivative, and

$$m_{0\rm e} = \sqrt{\frac{(k^2C_{\rm Se}^2-\omega^2)(k^2V_{\rm Ae}^2-\omega^2)}{(V_{\rm Ae}^2+C_{\rm Se}^2)(k^2C_{\rm Te}^2-\omega^2)}}, \tag{3}$$

where $C_{\rm Se}$ and $V_{\rm Ae}$ are the external acoustic and Alfvén speeds, respectively, and $C_{\rm Te} = \sqrt{\frac{V_{\rm Ae}^2C_{\rm Se}^2}{V_{\rm Ae}^2+C_{\rm Se}^2}}$ is the external tube speed. For the meanings of other parameters, please refer to Erdélyi & Fedun (2010).

In Equation (1), negative order $m$ is not allowed as $m = -1, -2, ...$ and $b = 0, -1, ...$ are the forbidden values of the denominatorial parameters of Kummer function (see 47:9 in Oldham et al. 2009). In this case, it may be approximately proportional to another Kummer function. When $m = -1$, $b = 0$ and $bM(a, b, x_0) \approx ax_0M(a + 1, 2, x_0)$. Equation (1) reduces to

$$D_{\rm e}\frac{r_0}{m_{0\rm e}}\frac{K_1(m_{0\rm e}r_0)}{K'_1(m_{0\rm e}r_0)} = -\frac{A^2r_0^2}{\mu_0^2} + D_{\rm i}r_0^2\frac{(1-\alpha^2)}{(\alpha-1)+2\frac{M(a+1,1,x_0)}{M(a+1,2,x_0)}}. \tag{4}$$

When $m = -2$, $b = -1$, $bM(a, b, x_0) \approx \frac{1}{2}M(a, 1, x_0)$ and $M'(a, b, x_0) = -aM(a+1, 0, x_0) \to \infty$. Equation (1) reduces to

$$D_e\frac{r_0}{m_{0\rm e}}\frac{K_1(m_{0\rm e}r_0)}{K'_1(m_{0\rm e}r_0)} = -\frac{A^2r_0^2}{\mu_0^2}. \tag{5}$$

On the other hand, Bennett et al. (1999) obtained an exact dispersion relation for wave propagation in incompressible twisted magnetic flux tubes, in which the modified Bessel functions $I_m$ and $K_m$ accept a negative order $m$. Therefore, no more efforts should be done to change it.

### 2.3 Stability of the Compressible Twisted Flux Tubes

We would like to check stability of the twisted flux tubes when they are disturbed slightly. In Equation (3), let $\omega^2 = 0$, then $m_{0\rm e} = k$. Now, $a \to \infty$ and $x_0 = \frac{1}{4}\frac{r_0^2k_\alpha^2}{a} \to 0$, where we have written

$$k_\alpha = k\sqrt{1-\alpha^2}, \tag{6}$$

$$\alpha^2 = \frac{4A^2}{\mu_0\rho_{0\rm i}\omega_{\rm Ai}^2}, \tag{7}$$

$$\omega_{\rm Ai} = \frac{A}{\sqrt{\mu\rho_{0\rm i}}}(m + kp), \tag{8}$$

$$p = \frac{B_{0z}}{A}. \tag{9}$$

Note that we have dropped $2\pi$ in the last equation that represents the pitch of the magnetic field. Then,

$$\lim_{a\to\infty, x_0\to 0} 2x_0\frac{M'(a,b,x_0)}{M(a,b,x_0)} = k_\alpha r_0\frac{I_{m+1}(k_\alpha r_0)}{I_m(k_\alpha r_0)}, \tag{10}$$

in Equation (1) and it becomes

$$D_{\rm e}\frac{r_0}{k}\frac{K_m(kr_0)}{K'm(kr_0)} = -\frac{A^2r_0^2}{\mu_0^2} + D_{\rm i}r_0^2\frac{(1-\alpha^2)}{m(1-\alpha)+k_\alpha r_0\frac{I_{m+1}(k_\alpha r_0)}{I_m(k_\alpha r_0)}}, \tag{11}$$

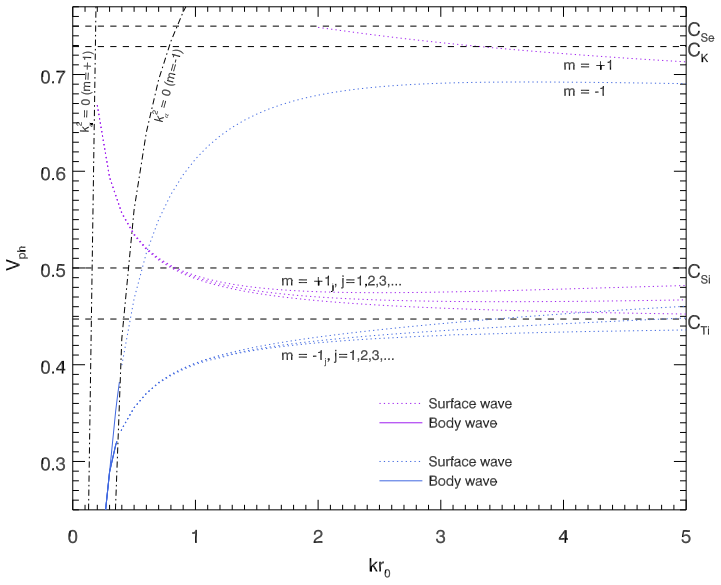


**Fig. 1** Under photospheric conditions ($C_{\rm Se}=0.75V_{\rm Ai}$, $V_{\rm Ae}=0.25V_{\rm Ai}$ and $C_{\rm Si}=0.5V_{\rm Ai}$, please see Erdélyi & Fedun 2010), the diagram curves of the dimensionless phase speed ($V_{\rm ph}$) of the kink ($m=\pm1$) modes as a function of the dimensionless wavenumber ($kr_0$) for a uniformly twisted intense magnetic flux tube ($V_{{\rm Ai}\phi}=0.1$). $C_{\rm K}$, $C_{\rm Si}$ ($C_{\rm Se}$) and $C_{\rm Ti}$ are the kink, sound and tube characteristic speeds on the photosphere. The *dot-dashed curves* correspond to the place where $k_\alpha^2=0(m=\pm1)$ in the plots. Their left-/right-side regions are the domains where only body ($k_\alpha^2<0$)/surface ($k_\alpha^2>0$) waves are present.

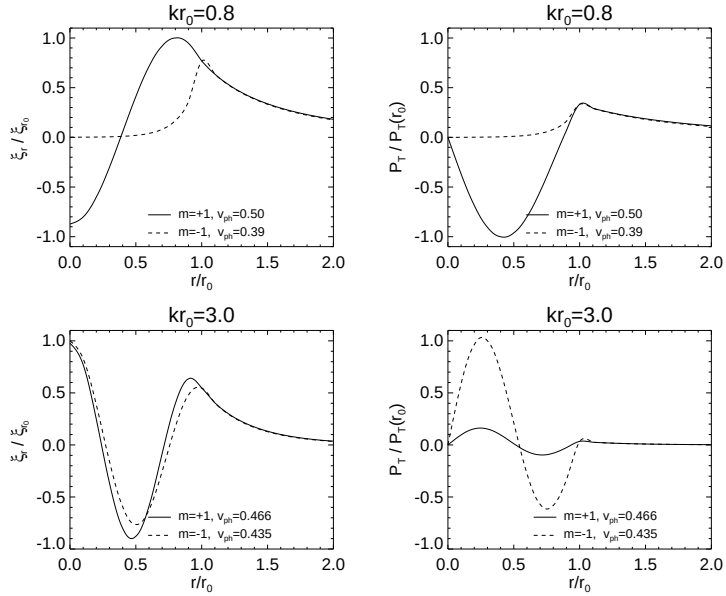


**Fig. 2** The normalised eigenfunctions $\xi_r/\xi_{r_0}$ (*left panels*) and $P_{\rm T}/P_{\rm T}(r_0)$ (*right panels*) of the kink $m=\pm1$ modes are plotted for the case of $C_{\rm Se}=0.75V_{\rm Ai}$, $V_{\rm Ae}=0.25V_{\rm Ai}$ and $C_{\rm Si}=0.5V_{\rm Ai}$ (photosphere conditions) when $V_{{\rm Ai}\phi}=0.1$ in a compressible medium.

where $D_{\rm e}=-\frac{1}{\mu_0}A^2(m+kp)^2$ and $D_{\rm i}=-\frac{1}{\mu_0}k^2B_{\rm e}^2$ as $\omega^2=0$. In form, the equation is consistent with the dispersion equation of the oscillation modes of a twisted magnetic flux tube in an incompressible medium (Erdélyi & Fedun 2010). We further define

$$\mathcal{K}_m=\frac{kr_0K_m'(kr_0)}{K_m(kr_0)},\chi_m=k_\alpha r_0\frac{I_{m+1}(k_\alpha r_0)}{I_m(k_\alpha r_0)}, \quad (12)$$

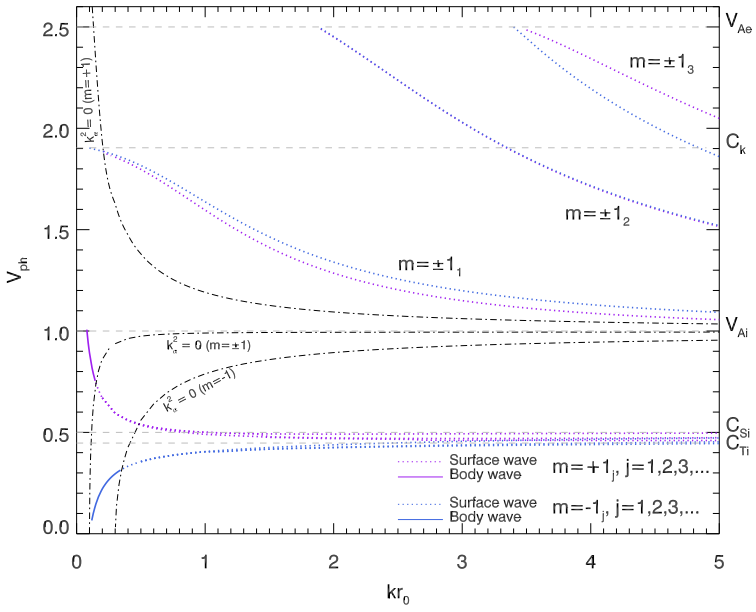


**Fig. 3** Under coronal conditions ($C_{\rm Se} = 0.25V_{\rm Ai}$, $V_{\rm Ae} = 2.5V_{\rm Ai}$ and $C_{\rm Si} = 0.5V_{\rm Ai}$, please see Erdélyi & Fedun (2010)), the diagram curves of the dimensionless phase speed ($V_{\rm ph}$) of the kink ($m = \pm 1$) modes as a function of the dimensionless wavenumber ($kr_0$) for a uniformly twisted intense magnetic flux tube ($V_{{\rm Ai}\phi} = 0.1$). $V_{\rm Ai}$ ($V_{\rm Ae}$), $C_{\rm K}$, $C_{\rm Si}$ ($C_{\rm Se}$) and $C_{\rm Ti}$ are the Alfvén, kink, sound and tube characteristic speeds on the corona. The *dot-dashed curves* correspond to the place where $k_\alpha^2 = 0$ in the plots. Note that the top one is for the $m = +1$ mode, the bottom for $m = -1$ mode and the middle for the both. For each mode ($m = +1$ or $m = -1$), the body ($k_\alpha^2 < 0$) waves only exist in between curves.

and Equation (10) becomes

$$[(m + kp)\chi_m + 2m][1 - (kr_0)^2 \frac{(B_{\rm e}/Ar_0)^2}{\mathcal{K}_m}] = 4(m + kp) - (m + kp)^3\,, \tag{13}$$

which is just equation (35) in Bennett et al. (1999). Therefore, their analyses about stability of the disturbed incompressible twisted flux tube is also suitable for the case of compressibility. They argued that $m = \pm 1$ are the most important modes and $m = 1$ is the most unstable of the two. In this case, for small $kr_0$ and $kp$, when the ratio of the external field to azimuth field is unless than $\frac{1}{2}$, that is $\frac{B_{\rm e}}{Ar_0} \geq \frac{1}{2}$, the tube is stable. In a following section, we only present the diagrams of dispersion relation for the $m = \pm 1$ modes.

## 3 DIAGRAMS OF THE DISPERSION RELATIONS

### 3.1 Compressibility

So far, the dispersion relation diagrams for the sausage ($m = 0$), kink ($m = 1$) and fluting ($m > 1$) modes have been extensively investigated, but those of their counterparts, the negative modes, are absent. We attempt to accomplish them and focus on the kink $m = \pm 1$ wave modes. In a compressible medium for the $m = +1$ mode, Erdélyi & Fedun (2010) demonstrated that under photosphere conditions, the fast kink surface mode has a cut-off at a phase speed $V_{\rm ph} = C_{\rm Se}$ that has no phase speed solution for small dimensionless wavenumbers, i.e. $kr_0 << 1$ when there is magnetic twist, and the phase speed $V_{\rm ph}$ of the slow kink surface mode tends to infinity as $kr_0 \to 0$ as shown in Figure 1. For the $m = -1$ mode, the figure shows that its phase speeds of both the slow and fast kink surface modes are less than those of the $m = +1$ mode, and the curves of the slow kink surface mode seem to be a mirror of the counterparts of the $m = +1$ mode relative to a speed slightly greater than $C_{\rm Ti}$. Moreover, there is a so-called mixed (hybrid) character at $kr_0 \approx 0.35$ for both the fast and slow surface kink modes, and their phase speed $V_{\rm ph}$ tends to zero as $kr_0 \to 0$. With $kr_0 \to 0$ the phase speed difference between the two modes of $m = \pm 1$ becomes more and more significant. However, this difference would become less and less significant with $kr_0$ increasing. In Figure 2, we plot the normalized eigenfunctions $\xi_r$ and $P_{\rm T}$ of the fundamental $m = \pm 1$ modes as a function of radius $r_0$. Comparing the left two panels, we can find that the phase speed difference between the two modes is larger and their difference in amplitude ($\xi_r$) is also larger. However, their difference in total pressure disturbance ($P_{\rm T}$) does not show such a similar change as shown in the right two panels.

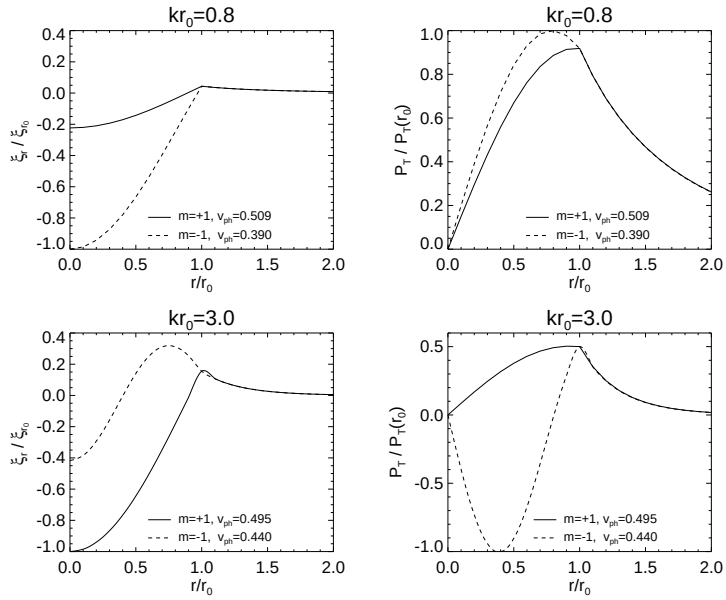


**Fig. 4** The normalised eigenfunctions $\xi_r/\xi_{r_0}$ (*left panels*) and $P_{\rm T}/P_{\rm T}(r_0)$ (*right panels*) of the kink $m = \pm 1$ modes are plotted for the case of $C_{\rm Se} = 0.25V_{\rm Ai}$, $V_{\rm Ae} = 2.5V_{\rm Ai}$ and $C_{\rm Si} = 0.5V_{\rm Ai}$ (coronal conditions) when $V_{Ai\phi} = 0.1$ in a compressible medium.

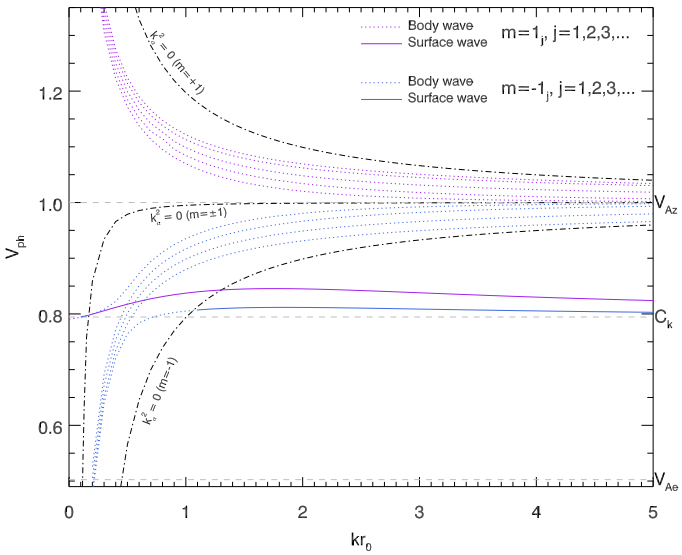


**Fig. 5** The diagram curves of the dimensionless phase speed ($V_{\rm ph}$) of the kink modes ($m = \pm 1$) as a function of the dimensionless wavenumber ($kr_0$) for an uncompressible twisted magnetic flux tube when $B_\theta = 0.1B_{0z}$ and $B_{\rm e} = 0.5\sqrt{B_{0z}^2 + B_\theta^2}$ (Bennett et al. 1999). $C_{\rm K}$ and $V_{\rm Ai}/V_{\rm Ae}$ are the kink and Alfvén characteristic speeds. The *dot-dashed curves* correspond to the place where $k_\alpha^2 = 0$ in the plots. Note that the top one is for the $m = +1$ mode, the bottom for $m = -1$ mode and the middle for the both. For each mode ($m = +1$ or $m = -1$), the body ($k_\alpha^2 < 0$) waves only exist in between curves.

These features will also appear in the following diagrams of dispersion relation. Under coronal conditions, as shown in Figure 3 the phase speed $V_{\rm ph}$ of the fast kink surface mode of $m = -1_1$ is slightly greater than that of the fast kink surface mode of $m = +1_1$, the two phase speeds of the fast kink surface mode of $m = \pm 1_2$ are equal in magnitude, and the phase speed $V_{\rm ph}$ of the fast kink surface mode of $m = -1_3$ is less than that of the fast kink surface mode of $m = +1_3$. The phase speeds of the fast kink surface modes of $m = \pm 1_{2,3}$ have a cut-off at a phase speed $V_{\rm ph} = V_{\rm Ae}$. For the slow kink surface modes, both the phase speed curves of the $m = \pm 1$ modes

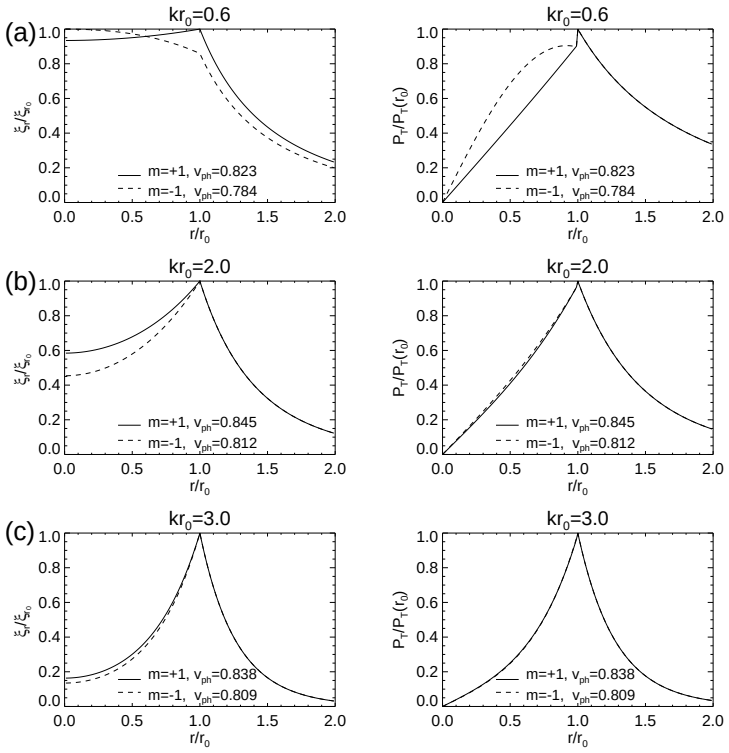


**Fig. 6** The normalised eigenfunctions $\xi_r/\xi_{r_0}$ (*left panels*) and $P_{\rm T}/P_{\rm T}(r_0)$ (*right panels*) of the kink $m = \pm 1$ modes are plotted for the case $B_\theta = 0.1B_{0z}$ and $B_{\rm e} = 0.5\sqrt{B_{0z}^2 + B_\theta^2}$ in an incompressible medium.

shows a mixed feature as $kr_0 \to 0$, of which the $m = +1$ mode tends to infinity while the $m = -1$ mode tends to zero. Moreover, the two sets of curves show symmetry in morphology relative to a speed slightly greater than $C_{\rm Ti}$. In Figure 4, we plot the normalized eigenfunctions $\xi_r$ and $P_{\rm T}$ of the fundamental $m = \pm 1$ modes as a function of radius $r_0$. It shows that the phase speed difference being large between the two modes does not mean that their differences in amplitude of $\xi_r$ and $P_{\rm T}$ are also large.

### 3.2 Incompressibility

In an incompressible medium, the sound speed tends to infinite and the slow-wave tube speed becomes the Alfvén speed. The fast waves are eliminated from the system and there is no distinction between the Alfvén continuum and the slow continuum (Bennett et al. 1999). Following Bennett et al. (1999), we take external field $B_{\rm e} = 0.5\sqrt{B_{0z}^2 + B_\theta^2}$ and $B_\theta = 0.1B_{0z}$. The dimensionless phase speed ($V_{\rm ph}$) of the kink modes ($m = \pm 1$) as function of the dimensionless wavenumber ($kr_0$) for an incompressible twisted magnetic flux tube are shown in Figure 5. The phase velocity bands of the body waves of $m = \pm 1$ show symmetry with respect to the Alfvén speed $V_{\rm Az}$. The $m = +1$ mode tends to infinity, while the $m = -1$ mode tends to 0 as $kr_0 \to 0$. The surface wave of $m = +1$ shows a mixed feature as $kr_0 \to 0$ and that of $m = -1$ shows the feature at $kr_0 \approx 1.1$. In Figure 6, we plot the normalized eigenfunctions $\xi_r$ and $P_{\rm T}$ of the fundamental $m = \pm 1$ modes as a function of radius $r_0$. It shows that the differences of $\xi_r$ and $P_{\rm T}$ between the modes decrease with their phase speed differences decreasing.

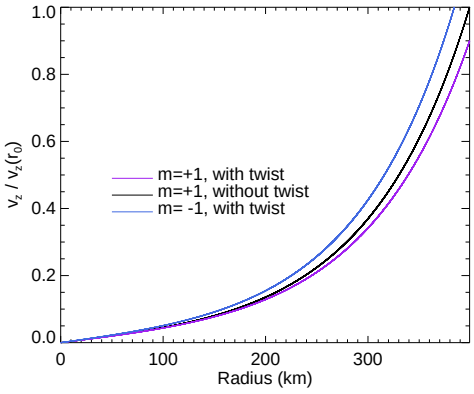


**Fig. 7** The normalised velocity component $v_z/v_z(r_0)$ of the kink $m = \pm 1$ wave modes as function of radius are plotted in an incompressible magnetic cylinder, of which the *blue*/*pink curves* are for the twisted cylinder and the *black curve* for the untwisted one.

**Table 1** Parameters of Nine Objects Observed by YFOSC

| Twist | $m$ | $C_{\rm Si}$ (m s$^{-1}$) | $C_{\rm Ai}$ (m s$^{-1}$) | $C_{{\rm Ai}\phi}$ (m s$^{-1}$) | $C_{\rm Ae}$ (m s$^{-1}$) | $C_{\rm Se}$ (m s$^{-1}$) | $T_{\rm ph}$ (s) | $\omega$ (rad s$^{-1}$) | $kr_0$ | $V_{\rm ph}$ (m s$^{-1}$) | $k_\alpha^2$ | $k$ ($10^{-6}$) | $r_0$ (km) | $d$ (km) |
|---|---|---|---|---|---|---|---|---|---|---|---|---|---|---|
| No | +1 | 9000 | 8182 | 818 | 2045 | 9818 | 150 | 0.042 | 3 | 5574 | $>0$ | 7.51 | 399 | 100 |
| Yes | +1 | 9000 | 8182 | 818 | 2045 | 9818 | 150 | 0.042 | 3 | 5724 | $>0$ | 7.32 | 410 | 100 |
| Yes | −1 | 9000 | 8182 | 818 | 2045 | 9818 | 150 | 0.042 | 3 | 5365 | $>0$ | 7.81 | 384 | 100 |

$T_{\rm ph}$ is period of the wave modes and $d$ is depth of the oscillation source under photosphere.

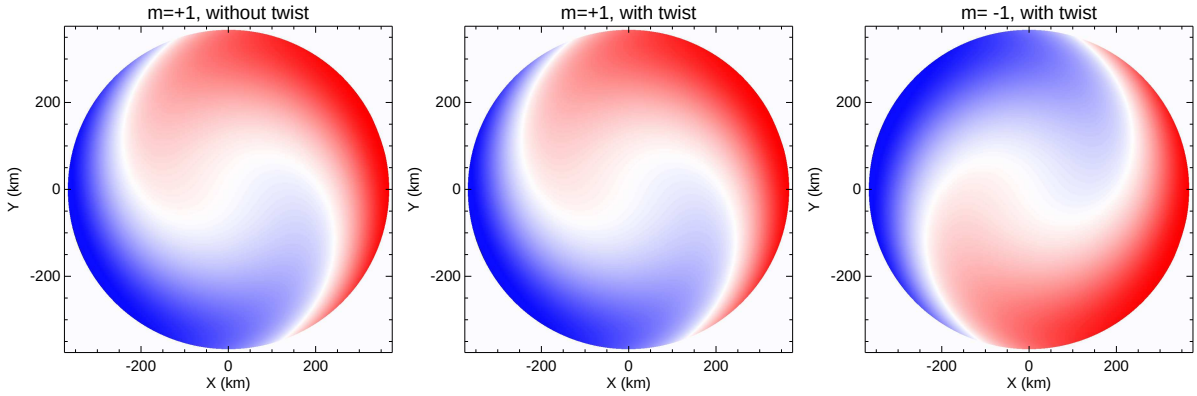


**Fig. 8** Snapshots of the simulated velocity component of $v_z$ for the kink $m = \pm1$ wave modes in $x - y$ plane. The left panel is for the untwisted magnetic cylinder and the middle and right ones for the twisted cylinder. An animation of this figure is available at *http://www.raa-journal.org/docs/Supp/ms4795fig8.mp4*.

## 4 MODELING OF SPIRAL WAVE PATTERNS

Kang et al. (2019) interpreted the spiral wave patterns (SWPs, Sych & Nakariakov 2014; Su et al. 2016; Sych et al. 2020) as the azimuthal wave modes ($m = 0, 1, 2$) propagating in an untwisted uniform magnetic cylinder. In this work, we follow their scenario and revisit the issue. The magnetic twist is added into the flux tube and the wave modes with $m = \pm1$ are investigated. The internally oscillatory solution (surface waves) of the longitudinal velocity is given as follows (Erdélyi & Fedun 2010)

$$v_z = -C_1 \left\{ \{kr_0 - \frac{V_{{\rm A}iz}V_{\rm ph}^2(mV_{{\rm A}i\phi} + kr_0V_{{\rm A}iz})}{V_{\rm ph}^2(C_{\rm Si}^2 + V_{\rm Ai}^2) - C_{\rm Si}^2V_{f_B}^2} \right. \\ \left. [1 - 2V_{{\rm A}i\phi}^2 \frac{m(1-\alpha) + \frac{2xM'(a,b,x)}{M(a,b,x)}}{k^2r_0^2(V_{\rm ph}^2 - V_{f_B}^2)(1-\alpha^2)}]\} \right\} \\ \times \frac{x^{\frac{m}{2}} \exp^{-\frac{x}{2}} M(a,b,x) \exp^{i(kz+m\phi-\omega t)}}{kr_0(V_{\rm ph}^2 - V_{f_B}^2)}, \quad (14)$$

where $C_1$ is arbitrary constant, $V_{\rm ph} = \omega/k$ is phase speed, $V_{{\rm A}iz}$ and $V_{{\rm A}i\phi}$ are the two components of the internal Alfvén speed $V_{\rm Ai}$ in the longitudinal and azimuth directions of the cylinder, respectively, $V_{\rm Si}$ is internal acoustic speed and

$$V_{f_B} = \sqrt{\frac{m^2V_{{\rm A}i\phi}^2}{k^2r_0^2} + \frac{2mV_{{\rm A}i\phi}V_{{\rm A}iz}}{kr_0} + V_{{\rm A}iz}^2}. \quad (15)$$

The phase speed $V_{\rm ph}$ is derived from the dispersion relations (1) and (3) for the wave modes of $m = \pm1$, respectively. Under photosphere conditions, we take $V_{\rm Ai} = 8182\,{\rm ms}^{-1}$, $C_{\rm Se} = 1.2V_{\rm Ai}$, $V_{\rm Ae} = 0.25V_{\rm Ai}$, $C_{\rm Si} = 1.1V_{\rm Ai}$, and $V_{{\rm A}i\phi} = 0.1V_{\rm Ai}$. Table 1 lists all the relevant parameters related to the wave modes of $m = \pm1$ propagating in the twisted magnetic cylinder. For comparison, the $m = +1$ wave mode in untwisted cylinder is also included in the table. As $k_\alpha^2 > 0$ for the listed three modes, they are all surface waves which decay away from the cylinder's surface.

Figure 7 shows the normalized $v_z$ as function of the radius of cylinder for the $m = \pm1$ wave modes in a twisted flux tube and $m = +1$ in an untwisted flux tube. At a fixed radius value, the value of $m = +1$ wave mode in the untwisted flux tube is less/greater than that of $m = -1/m = +1$ wave mode in the twisted flux tube. Figure 8 shows $v_z$ maps of the $m = \pm1$ wave modes emerging from a depth of $d = 100$ km under photosphere. The $m = \pm1$ wave modes have an opposite phase relation. In morphology, there is no significant difference between the wave modes of $m = +1$ in the twisted and untwisted magnetic cylinders. It indicates that the magnetic twist has no great influence on the morphology of SWPs in the frame of linear perturbation analysis. We can suppose that the complex structure of magnetic field in the sunspot with different cutoff frequencies along different polar angles play a major role in forming SWPs. Waves propagating

radially along magnetic waveguides will lead to their frequency fragmentation and the appearance of a quasi-spiral spatial shape.

## 5 CONCLUSIONS

In this work, based on the work of Erdélyi & Fedun (2010) we derive the dispersion equation for the $m = -1$ magneto-acoustic wave mode in the compressible magnetized twisted flux tubes. We find that the analyses about stability of the incompressible twisted flux tube are also suitable for the case of compressibility. $m = \pm 1$ are the most important modes and $m = 1$ is the more unstable of the two. We then present a complete dispersion relationship diagram that includes both the magnetic twist and the negative order $m = -1$. Furthermore, we revisit the issue of spiral wave patterns in sunspot and find that there is no obvious difference in the morphologies of umbral spiral waves with and without magnetic twist. The main results for the magneto-acoustic waves in magnetic twisted flux tubes are summarized as follows.

(1) Under photosphere conditions, the azimuthal $m = \pm 1$ wave modes show great difference in phase-speed at finite $kr_0$ for both the fast and slow mode waves. This difference tends to decrease with $kr_0$ increasing.

(2) Under coronal conditions, the azimuthal $m = \pm 1$ wave modes show great difference in phase-speed at finite $kr_0$ only for the slow mode waves, while for the fast mode waves they show a finite difference no more than $10\%$ at the allowed values of $kr_0$ for the first harmonic curves ($m = \pm 1_1$).

(3) The magnetic twist may has no great influence on the morphology of SWPs in the frame of linear perturbation analysis. We think that the spatial and frequency fragmentation of wavefronts as the combination of narrowband spherical and linear parts of the wavefronts can provide the observed spirality. The study of relationship between wave shapes and maps of the magnetic field inclination angles presented in Sych et al. (2020) confirms this assumption.

**Acknowledgements** We are grateful to an anonymous referee for constructive suggestions. This work is supported by the Strategic Priority Research Program on Space Science, the Chinese Academy of Sciences (Grant Nos. XDA15320302, XDA15052200 and XDA15320102), National Natural Science Foundation of China (Grant Nos. 11773038, U1731241 and 11427803), and the 13th Five-year Informatization Plan of the Chinese Academy of Sciences (Grand No. XXH13505-04). RS research was performed within the basic funding from FR program II.16, RAS program KP19-270, and supported by the Chinese Academy of Sciences President's International Fellowship Initiative (Grant No. 2020VMA0032).

## References

Bennett, K., Roberts, B., & Narain, U. 1999, Sol. Phys., 185, 41
Edwin, P. M. & Roberts, B. 1983, Sol. Phys., 88, 179
Erdélyi, R. & Fedun, V. 2006, Sol. Phys., 238, 41
Erdélyi, R. & Fedun, V. 2007, Sol. Phys., 246, 101
Erdélyi, R. & Fedun, V. 2010, Sol. Phys., 263, 63
Kang, J., Chae, J., Nakariakov, V. M., et al. 2019, ApJL, 877, L9
Oldham, K., Myland, J. & Spanier, J. 2009, An Atlas of Functions (2nd. New York: Springer)
Su, J. T., Ji, K. F., Cao, W., et al. 2016, ApJ, 817, 117
Sych, R. & Nakariakov, V. M. 2014, A&A, 569, A72
Sych, R., Jess, D. B., & Su, J. 2020, Phil. Trans. R. Soc. A, 379, 20200180